Low-temperature galvanomagnetic, magnetic, and thermoelectric properties of Mo3Sb7−xTex (x = 0.0 , 0.3, 1.0, 1.6, and 1.8)

Christophe Candolfi, Bertrand Lenoir, Anne Dauscher, Jiří Hejtmánek, Janusz Tobola

Low-temperature galvanomagnetic, magnetic, and thermoelectric properties of $Mo_3Sb_{7-x}Te_x$ ($x=0.0$, 0.3, 1.0, 1.6, and 1.8)

C. Candolfi,*,† B. Lenoir, and A. Dauscher
Institut Jean Lamour, UMR CNRS-Nancy Université-UPVM 7198, Ecole Nationale Supérieure des Mines de Nancy, Parc de Saurupt, 54042 Nancy Cedex, France

J. Hejtmánek
Institute of Physics, Academy of Sciences of the Czech Republic, Cukrovarnicka 10, CZ-162 53 Praha 6, Czech Republic

J. Tobola
Faculty of Physics and Applied Computer Science, AGH University of Science and Technology, 30-059 Krakow, Poland
(Received 25 March 2009; revised manuscript received 30 April 2009; published 4 June 2009)

The galvanomagnetic, thermoelectric, and magnetic properties of some polycrystalline $Mo_3Sb_{7-x}Te_x$ compounds ($x=0.0$, 0.3, 1.0, 1.6, and 2.2) have been experimentally investigated from 2 to 350 K. These samples were prepared via a metallurgical route, and characterized by x-ray diffraction and electron probe microanalysis. Experiments were completed by theoretical information including dispersion curves, and total and partial densities of states within the framework of the Korringa-Kohn-Rostoker method with the coherent-potential approximation. These theoretical aspects have highlighted a shift of the Fermi level toward the valence-band edge with increasing x that can be understood within a rigid-band model. Transport property measurements have not only provided compelling evidence for this picture but have also shown that their variations with the Te content is consistent with a progressive crossover from a metalliclike to a semiconductinglike state as theoretically suggested. The enhancement of the thermal conductivity as x increases constitutes one of the most impressive properties of this system. This surprising behavior is tentatively ascribed to the disappearance of a strong scattering of phonons by magnetic excitations displayed by Mo_3Sb_7. The compositional evolution of the magnetic properties has brought further evidence of a progressive suppression of these magnetic excitations as the Te concentration increases. In addition, magnetic susceptibility together with specific-heat measurements have confirmed the decrease in the total density of states at the Fermi level with x suggested by our band-structure calculations.

DOI: 10.1103/PhysRevB.79.235108 PACS number(s): 72.20.Pa

I. INTRODUCTION

A resurgence of interest in the search for highly efficient thermoelectric materials has been witnessed in the last fifteen years. The essence of a good thermoelectric material is contained in the dimensionless figure of merit, ZT, given at a temperature T and expressed as $ZT=\alpha^2T/\rho\lambda$, where α is the Seebeck coefficient or thermopower, ρ is the electrical resistivity, and λ is the total thermal conductivity composed of two terms: the lattice thermal conductivity λ_L and the carrier thermal conductivity λ_e.[1] To maximize the ZT value requires a judicious balance of both the thermal and electrical properties to synthesize a solid that can conduct heat like a glass but that can also maintain the good electrical properties associated with doped semiconducting crystals.[2]

Extensive efforts are currently undertaken to find materials with complex crystalline structure or having weakly bounded atoms in oversized atomic cages.[3–7] Both features are believed to cause a strong scattering of the heat-carrying lattice waves, e.g., to dramatically decrease the lattice thermal conductivity. The challenge then lies in trying to maintain low electrical resistivity and high Seebeck coefficient values.

Recent studies show that the M_3T_7 compounds (with M =Nb, Mo, Tc, Re, Ru, Os, Ir, Co, Ni, Pd, and Pt, and T =Sb, Te, As, Sn, Si, Al, Ga, Ge, In, Pb, and Tl),[8,9] crystallizing in the cubic Ir_3Ge_7 structure type (space-group $Im3m$), could stand as prime candidates for thermoelectric applications at high temperature.[10,11] The crystallographic structure of these materials can be described either by a three-dimensional arrangement of antiprisms formed by T atoms, with the M atoms sitting at the center of these elementary building blocks, or by two interpenetrating sublattices composed by the M and T atoms. The electronic structure of some of these compounds is characterized by an energy gap near the Fermi level arising from a strong d-p orbitals hybridization.[8] Among the twenty five compounds discovered up to now, two members of this family were found to display this feature, namely, Re_3As_7 and Mo_3Sb_7.[8] While the latter compound has received great attention due to intriguing physical features such as superconducting properties and a spin gap formation at $T^*=53$ K,[12–21] both materials were found to exhibit metallic properties preventing to attain high ZT values. However, band-structure calculations have shown that the Fermi levels are positioned near the band gap. Hence, the addition of either one hole to Re_3As_7 or two electrons to Mo_3Sb_7 per formula unit could drive the Fermi level into the gap. Besides a rigidlike behavior of the electronic structure, such a shift would then imply a crossover from a metallic to a semiconducting regime of conduction. These assumptions were experimentally investigated by substituting As and Sb atoms by Ge and Te atoms, respectively.

Even if a semiconducting state could not be reached in the $Mo_3Sb_{7-x}Te_x$ system due to a solubility limit of Te lower than the required value, the thermoelectric performances were found to be greatly improved with a maximum *ZT* value of ~0.8 at 1050 K for $x=1.6$.[11,22] Even though the $Mo_3Sb_{7-x}Te_x$ compounds possess optimum thermoelectric properties at high-temperature, low-temperature measurements can provide useful and essential information regarding the influence of Te on the thermal and electronic properties. To shed light on the microscopic mechanisms dominating thermal and electrical conductions is therefore essential to optimize the thermoelectric properties of Mo_3Sb_7.

To carry out this study, polycrystalline $Mo_3Sb_{7-x}Te_x$ samples with nominal concentrations of $x=0.0$, 0.3, 1.0, 1.6, and 2.2 have been synthesized. Here, we report on both experimental and theoretical results including thermal conductivity, thermopower, electrical resistivity, Hall effect, magnetization, specific-heat measurements, as well as electronic band-structure calculations. The "rigidlike" behavior of the electronic structure, the disappearance of the magnetic interactions and the thermoelectric properties dependence as the Te content increases constitute the outstanding issues we address in the present paper.

II. EXPERIMENTAL AND COMPUTATIONAL DETAILS

Polycrystalline samples of $Mo_3Sb_{7-x}Te_x$ with $x=0.0$, 0.15, 0.3, 1.0, 1.6, and 2.2 were prepared via the following metallurgical route. Stoichiometric amounts of high-purity Sb shots (99.999%), Mo powder (99.999%), and Te shots (99.999%) were loaded into a quartz ampoule in an argon-atmosphere glove box. The ampoule was heated up to 750 °C and left at this temperature for 10 days. To ensure good homogeneity, the grown ingots were then ground in an agate mortar into fine powders (<100 μm) that were cold pressed. The pellets were annealed at 750 °C for 15 days, then powdered again, and finally densified by hot pressing using graphite dies in an argon atmosphere at 600 °C for 2 h under 51 MPa. Structure and chemical composition were checked by x-ray diffraction (XRD), neutron diffraction, and electron probe microanalysis (EPMA). To obtain accurate lattice parameters by XRD, high-purity silicon was added as an internal standard.

Transport, magnetotransport, and magnetic measurements were carried out on parallelepipedic shaped samples cut from the hot pressed ingots with a diamond wire saw to typical dimensions of $2\times2\times10$ mm^3. Magnetotransport measurements were performed with an ac transport measurement system option (PPMS-Quantum Design) over the 2–350 K temperature range and under a magnetic field up to 7 T. Four-probe electrical resistivity, steady-state thermoelectric power, and thermal-conductivity measurements were realized from 3.5 to 300 K using an automated closed-cycle refrigerator system. Isothermal magnetization curves were measured from 5 to 300 K in applied fields of up to 7 T using a Quantum Design magnetometer (MPMS-Quantum Design). Specific-heat measurements were carried out on some selected samples in the 2–300 K temperature range using a Quantum Design PPMS setup.

Electronic structure calculations of $Mo_3Sb_{7-x}Te_x$ ($0.0\leq x\leq2.0$) were performed by the Korringa-Kohn-Rostoker (KKR) method with the coherent-potential approximation (CPA) to treat the chemical disorder.[23,24] The self-consistent crystal potential of the muffin-tin form was constructed within the local-density approximation (LDA) applying the von Barth-Hedin formula for the exchange-correlation part. The experimental lattice and atomic coordinates determined for the $x=0.0$ and $x=1.6$ samples from neutron-diffraction experiments were linearly extrapolated throughout the 0.0–2.0 concentration range to perform these computations.[25] Since previous investigations based on total-energy KKR-CPA LDA calculations coupled with neutron diffraction analyses have unequivocally shown that the Te atoms exhibit a strong site preference for the Sb1 position (12*d* site).[25] This kind of chemical Sb-Te disorder was taken into account. Energy dispersion curves along high-symmetry directions in the bcc Brillouin zone were also calculated for the illustrative $x=1.6$ compound. For final crystal potentials and atomic charges (converged below 1 mRy and $10^{-4}e$, respectively), total, site-decomposed, and *l*-decomposed densities of states (DOS) were computed using a dense energy point's mesh to allow precise numerical derivation of the DOS to further estimate the thermopower. Since the Fermi energy E_F is of prime importance to determine the DOS value at E_F, it was computed from the generalized Lloyd formula and converged below 0.1 mRy for all compounds.[24]

III. RESULTS AND DISCUSSION

A. Structural and chemical characterizations

The XRD study has shown that all prepared samples display all the peaks characteristic of the Ir_3Ge_7 structure type (space-group $Im3m$). No trace of other phases could be detected in the Te substituted compounds for $x\leq1.6$ whereas a small amount of Sb and $MoTe_2$ were found in the $x=0.0$ and $x=1.8$ samples, respectively.[21] These results were further confirmed by EPMA which revealed that all the samples are homogeneous with actual compositions close to the nominal compositions except for the $x=2.2$ sample for which the actual concentration of Te was found to be $x\sim1.8$. As already noticed by Gascoin *et al.*[11] who found a maximum Te content of $x\sim1.7$, the solubility limit of Te in the Mo_3Sb_7 compound is lower than the theoretical limit ($x=2.0$) required to achieve semiconducting properties. All the compositions were normalized to full occupancy of the molybdenum site. Figure 1 shows the variation in the lattice parameter, which linearly decreases with increasing Te concentration following Vegard's law. In Table I are summarized the lattice parameters of the different samples, the actual chemical compositions as determined from EPMA, and the relative densities defined as the ratio of the measured density to the theoretical density. In this paper, the actual compositions will always be used.

B. Band-structure calculations

The variation in the total DOS of the $Mo_3Sb_{7-x}Te_x$ compounds ($0.0\leq x\leq2.0$) versus Te concentration is plotted in

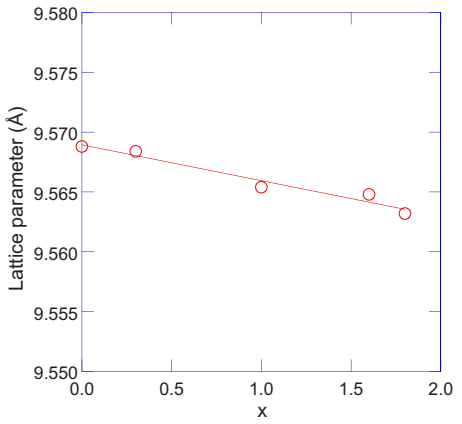

FIG. 1. (Color online) Lattice parameter of $Mo_3Sb_{7-x}Te_x$ as a function of the Te content as determined from XRD analyses. The x values correspond to the actual compositions obtained by EPMA.

Fig. 2. Noteworthy, the full potential KKR calculations recently reported for Mo_3Sb_7 (Refs. 19 and 21) led to a computed total DOS at the Fermi-level $[N(E_F)]$ value slightly smaller (141 states Ry^{-1} f.u.$^{-1}$) than that obtained from the KKR-CPA method (166 states Ry^{-1} f.u.$^{-1}$). This discrepancy, which presumably arises from the crystal potential, is not surprising given that the Fermi level is positioned in a region where a strong varying DOS slope is observed. The decrease in $N(E_F)$ with x is highly nonlinear for high Te contents ($1.6<x<2.0$) while it displays a quasilinear dependence for $0.0<x<1.6$. As evidenced in Fig. 2, the KKR-CPA $N(E_F)$ values closely correspond to those obtained by progressively shifting the Fermi level of Mo_3Sb_7 to the valence-band edge. These results strongly suggest a rigidlike behavior of the electronic structure as x is increased. Whatever the Te fraction is, it is interesting to notice that the Sb1 atoms contribution to $N(E_F)$ is found to be slightly larger than that of the Sb2 atoms (Table II) due to stronger electronic interactions on the latter site. Moreover, the decrease in $N(E_F)$ mainly arises from the decrease in the d-Mo contribution leading to lower Stoner product as the Te concentration increases (Table II).

As revealed by these KKR-CPA calculations, the Fermi level falls into the gap for $x=2.0$ and all atomic contributions vanish (Fig. 2). These results support the previous LMTO (linear muffin tin orbital) calculations performed in the orthorhombic approximant $Mo_3Sb_5Te_2$.[10] Further theoretical calculations show that, for higher Te concentration ($x>2.0$),

TABLE I. EPMA results, lattice parameter (a), and relative density (d) of the $Mo_3Sb_{7-x}Te_x$ compounds.

Nominal composition	EPMA	a (Å)	d (%)
Mo_3Sb_7	$Mo_3Sb_{6.95}$	9.568(8)	93
$Mo_3Sb_{6.7}Te_{0.3}$	$Mo_3Sb_{6.7}Te_{0.3}$	9.568(4)	95
Mo_3Sb_6Te	Mo_3Sb_6Te	9.565(4)	96
$Mo_3Sb_{5.4}Te_{1.6}$	$Mo_3Sb_{5.4}Te_{1.6}$	9.564(8)	90
$Mo_3Sb_{4.8}Te_{2.2}$	$Mo_3Sb_{5.2}Te_{1.8}$	9.563(3)	97

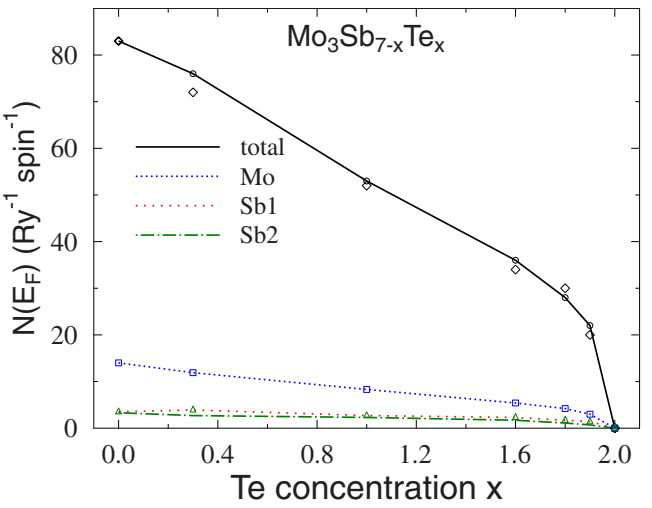

FIG. 2. (Color online) Variation in the KKR-CPA total and partial densities of states with Te concentration in the $Mo_3Sb_{7-x}Te_x$ system. To underline the rigidlike behavior of the electronic structure when x increases, values obtained by simply shifting the Fermi level of Mo_3Sb_7 toward the valence-band edge are shown by open-diamond symbols.

the Fermi level is expected to cross the energy gap and thus, a changeover from p-type to n-type conduction occurs. Dashjav *et al.*[10] showed that, for $x=2.3$, the compound still displays hole conduction with high Seebeck coefficient, in clear contradiction with our results. This discrepancy suggests that the actual Te fraction in their samples might be markedly different from the nominal concentration.

Figure 3 shows that the Fermi level of the ordered and disordered systems ($x=0.0$, 1.0, 1.6, and 1.8) lies in the physically interesting region since strong modifications of $N(E_F)$ and to a less extent its energy derivative $dN/dE|_{E_F}$ occur. As expected within a rigid-band model, a high Te concentration does not seem to exert strong influence on the shape of the valence bands.

A shift of the Fermi level to the valence-band edge should be related to a decrease in the carrier concentration leading to a concomitant increase in the electrical resistivity and thermopower. To examine more precisely this last assumption, the analysis of the DOS derivative can allow us to estimate the linear term of the thermopower, α/T, extrapolated to $T=0$ K, using the Mott's formula and assuming that the electrical conductivity is mainly driven by $N(E_F)$ (the carrier mobility is taken to be constant with energy). The calculated values of the thermopower at 100 K are listed in Table II and, as expected, increase with the Te content. However, we can anticipate that these values should tend to be overestimated with regard to the experimental values as it was already notified in recent calculations in some half-Heusler systems.[26] A better agreement between experimental and theoretical values can be obtained if both electrical resistivity and thermopower slopes are calculated via integration in the reciprocal space. Such more accurate treatment requires complete information on k-dependent electron velocities and lifetimes in the vicinity of the Fermi surface. These calculations are however difficult to undertake in the present case because of the complex Fermi surface displayed by Mo_3Sb_7.[14] Finally,

TABLE II. KKR-CPA computational results in the $Mo_3Sb_{7-x}Te_x$ compounds. Total and site-decomposed DOSs at E_F as well as thermopower values evaluated at 100 K are expressed in states Ry^{-1} f.u.$^{-1}$, states Ry^{-1} atom^{-1}, and $\mu V\ K^{-1}$, respectively. The Stoner product $I_{Mo}N_{Mo}(E_F)$, where I_{Mo} is the exchange integral ($I_{Mo} \sim 0.027$ Ry in the present case) and $N_{Mo}(E_F)$ is the partial density of states at the Fermi level of the Mo atoms, are also given. The experimental Seebeck coefficients (at 100 K) are given in parenthesis.

Chemical formula	$N_{tot}(E_F)$	$N_{Mo}(E_F)$	$N_{Sb1}(E_F)$	$N_{Te1}(E_F)$	$N_{Sb2}(E_F)$	$I_{Mo}N_{Mo}(E_F)$	S_{100}
Mo_3Sb_7	166	28.0	7.0	3.4	6.6	0.75	
$Mo_3Sb_{6.7}Te_{0.3}$	152	25.0	7.8	3.8	5.4	0.64	11 (8)
Mo_3Sb_6Te	106	16.6	5.4	2.6	4.6	0.45	16 (12)
$Mo_3Sb_{5.4}Te_{1.6}$	72	10.8	4.8	2.0	3.4	0.30	33 (19)
$Mo_3Sb_{5.2}Te_{1.8}$	56	8.4	3.4	1.2	2.2	0.23	35 (22)

we depict in the Fig. 4 the real part of the energy dispersion curve $E(\mathbf{k})$ of the illustrative $x=1.6$ sample. As we can clearly observe, the Fermi level is positioned in the vicinity of flat valence bands, suggesting high effective masses of the charge carriers.

C. Magnetic properties

At the heart of the issue of the transport properties variations in the $Mo_3Sb_{7-x}Te_x$ system is the evolution of the magnetic interactions exhibited by Mo_3Sb_7 as x progressively increases.[14,21] These interactions are related to antiferromagnetically coupled molybdenum dimers that lead to a spin gap formation at $T^*=53$ K. If the signature of this magnetic transition can be clearly observed on the low-temperature transport properties, the magnetic interactions displayed by Mo_3Sb_7 above T^* markedly influence the thermal transport both at low and high temperatures.[14,21] Magnetic-susceptibility measurements can thus provide pertaining issues to elucidate the variations in these interactions as x is enhanced as well as preliminary insights into the variations in $N(E_F)$ with the Te content. Figure 5 shows the variation in the magnetic susceptibility, χ, as a function of the temperature. For all Te substituted compounds, the χ values have been carefully derived from the slope of the isothermal magnetization curves after subtracting the temperature-independent ferromagnetic contribution that saturates at small fields. As previously reported, the pure Mo_3Sb_7 compound synthesized from the present metallurgical route does not exhibit any ferromagnetic contribution.[12] In addition, whatever the sample is, no temperature-dependent Curie-Weiss component could be evidenced in the whole temperature and magnetic-field ranges investigated. As evidenced in Fig. 5, the temperature dependences of the magnetic susceptibility of the $x=0.3$ and 1.0 samples are reminiscent to that observed for the parent Mo_3Sb_7 compound, and attributed to the molybdenum dimers and spin gap formation.[12,14] This evolution suggests that the magnetic interactions are still present, but to a less extent, in these compounds. At low temperature, the observed increase is likely related to the presence of paramagnetic impurities. Higher Te contents markedly affect this dependence since both the $x=1.6$ and 1.8 samples exhibit linear temperature dependence with a changeover from positive to negative values near 40 and 300 K, respectively. The higher magnetic-susceptibility values displayed by the latter sample are likely due to the contribution of paramagnetic secondary phases ($MoTe_2$).

The evolution of χ with the Te content strongly supports a progressive crossover from a paramagnetic metal to a diamagnetic semiconductor. However, the measured magnetic susceptibility of the $x=1.6$ sample is still significantly higher than the intrinsic diamagnetic contribution expected in a semiconducting state (evaluated to be $\sim -330\times10^{-6}$ emu mol^{-1} per formula unit using Pascal's constants[27,28]).

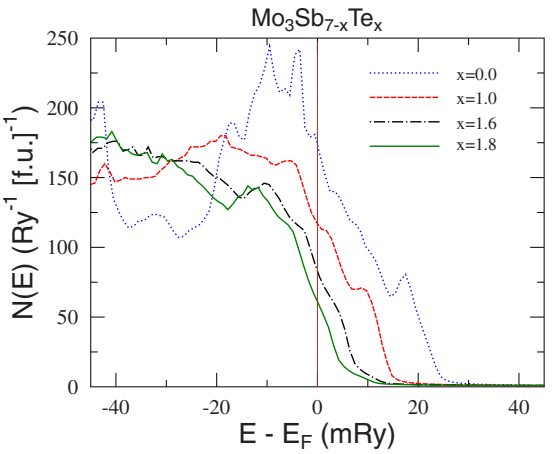

FIG. 3. (Color online) Total density of states as a function of the energy in the vicinity of the Fermi energy (vertical line) in $Mo_3Sb_{7-x}Te_x$ for $x=0.0$, 1.0, 1.6, and 1.8.

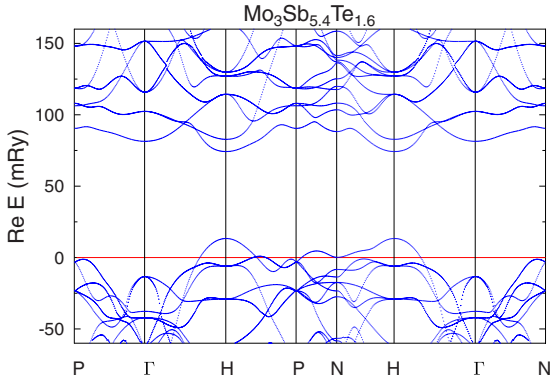

FIG. 4. (Color online) Dispersion curves along high-symmetry directions of the $x=1.6$ sample.

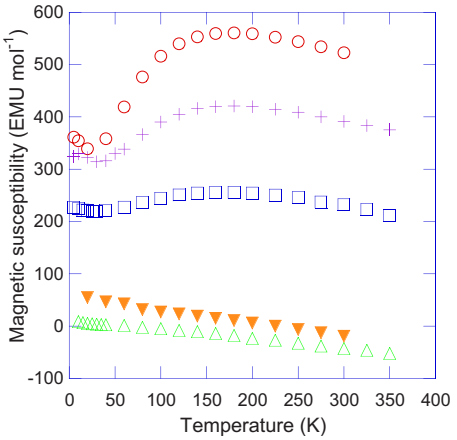

FIG. 5. (Color online) Temperature dependence of the molar magnetic susceptibility of the $Mo_3Sb_{7-x}Te_x$ substituted compounds for x=0.0 (○), 0.3 (+), 1.0 (□), 1.6 (△), and 1.8 (▼).

This fact, likely related to the paramagnetic contribution of the free carriers, is consistent with our KKR-CPA calculations and independently confirms that the Fermi level is not yet positioned into the gap. In addition, the temperature dependences of the magnetic susceptibility stand for compelling evidence of a suppression of the molybdenum dimer's magnetic interactions with increasing the Te concentration.

Considering the metallic nature of the samples, the low-temperature magnetic-susceptibility data can also be considered as a direct probe of the evolution of $N(E_F)$ with x. The magnetic susceptibility of the different samples studied can be thus written as

$$\chi = \chi_{\text{Pauli}} + \chi_{\text{dia}}, \tag{1}$$

where χ_{Pauli} is the Pauli susceptibility related to the susceptibility of the charge carriers subsystem and χ_{dia} the core diamagnetism of the constituent species. This last term can be evaluated using Pascal's constants and can then be subtracted to the measured magnetic susceptibility to estimate χ_{Pauli} for $T \rightarrow 0K$.[27,28] It is worth mentioning that, in the case of the x=0.0, 0.3, and 1.0 samples, because of the low temperature upturn related to paramagnetic impurities, a fit to the data (not shown) has been performed to subtract this parasitic contribution. The experimental values of $N(E_F)$ can be deduced from the χ_{Pauli} values supposing validity of the free-electron formula[29]

$$\chi_{\text{Pauli}} = N\mu_B^2 N(E_F) = 2.376 \times N(E_F), \tag{2}$$

where N is the number of electrons per mole of formula unit and μ_B is the Bohr magneton. In Eq. (2), χ_{Pauli} and $N(E_F)$ are expressed in 10^{-6} emu mol^{-1} and states Ry^{-1}, respectively. The values of the diamagnetic contribution χ_{dia} together with the Pauli susceptibility and the experimental $N(E_F)$ values are summarized in Table III. As we can easily appreciate, $N(E_F)$ progressively decreases as the Te content is enhanced, supporting our KKR-CPA calculations. The experimental Pauli susceptibility combined with theoretical $N(E_F)$ values also offer the opportunity to estimate the reduced effective masses of the charge carriers m^*/m_0 using the relation[29]

$$\chi_{\text{Pauli}} = \left(\frac{m^*}{m_0} - \frac{1}{3}\frac{m_0}{m^*}\right)\chi_{\text{Pauli}}^{\text{KKR-CPA}}, \tag{3}$$

where $\chi_{\text{Pauli}}^{\text{KKR-CPA}}$ is the theoretical Pauli susceptibility term inferred from KKR-CPA calculations [Eq. (2)]. This approach yields to high values of m^*/m_0 (Table III) and small variations against Te content. Such reduced effective masses may be related to high thermopower values in the $Mo_3Sb_{7-x}Te_x$ system.

D. Specific heat

As specific heat, C_p, can provide further evidence substantiating a decrease in $N(E_F)$ as well as relevant information on the lattice dynamics, we performed such experiments in the 2–300 K temperature range on the x=0.0 and 1.6 samples. Figure 6(a) shows the low-temperature specific-heat data, C_p/T, plotted as a function of T^2. A first essential outcome of these measurements lies in the disappearance of the superconducting transition exhibited by Mo_3Sb_7 at $T_c \sim 2.3$ K.[12–20] This suggests a decrease in the electron-phonon coupling strength with x. In addition, as clearly evidenced, the x=1.6 sample displays a perfect linear dependence over a broader temperature range (2–20 K, Fig. 6(b)), i.e., up to a significantly higher temperature than the binary compound (2.3–6 K). This main difference may be related to a depression of additional excitations such as magnetic fluctuations and/or to anharmonicity due to Te substitution. Supposing that the observed behavior mainly originates from the anharmonic contribution, we attempted to fit these low-temperature regions according to the relation

TABLE III. Values of the theoretical $[N(E_F)_{\text{KKR-CPA}}]$ and experimental $[N(E_F)_{\text{exp}}]$ total DOSs, the diamagnetic contribution χ_{dia}, and the Pauli susceptibilities inferred from both experimental data (χ_{Pauli}) and band-structure calculations ($\chi_{\text{Pauli}}^{\text{KKR-CPA}}$), and the derived values of the reduced effective masses m^*/m_0 using Eq. (3) for the x=0.0, 0.3, 1.0, and 1.6 compounds.

Chemical formula	$N(E_F)_{\text{KKR-CPA}}$ (states Ry^{-1} f.u.$^{-1}$)	$\chi_{\text{Pauli}}^{\text{KKR-CPA}}$ (emu mol^{-1})	χ_{dia} (emu mol^{-1})	χ_{Pauli} (emu mol^{-1})	$N(E_F)_{\text{exp}}$ (states Ry^{-1} f.u.$^{-1}$)	m^*/m_0
Mo_3Sb_7	166	395	280	650	261	1.8
$Mo_3Sb_{6.7}Te_{0.3}$	152	361	290	600	252	1.8
Mo_3Sb_6Te	106	252	310	530	231	2.2
$Mo_3Sb_{5.4}Te_{1.6}$	72	171	330	340	145	2.0

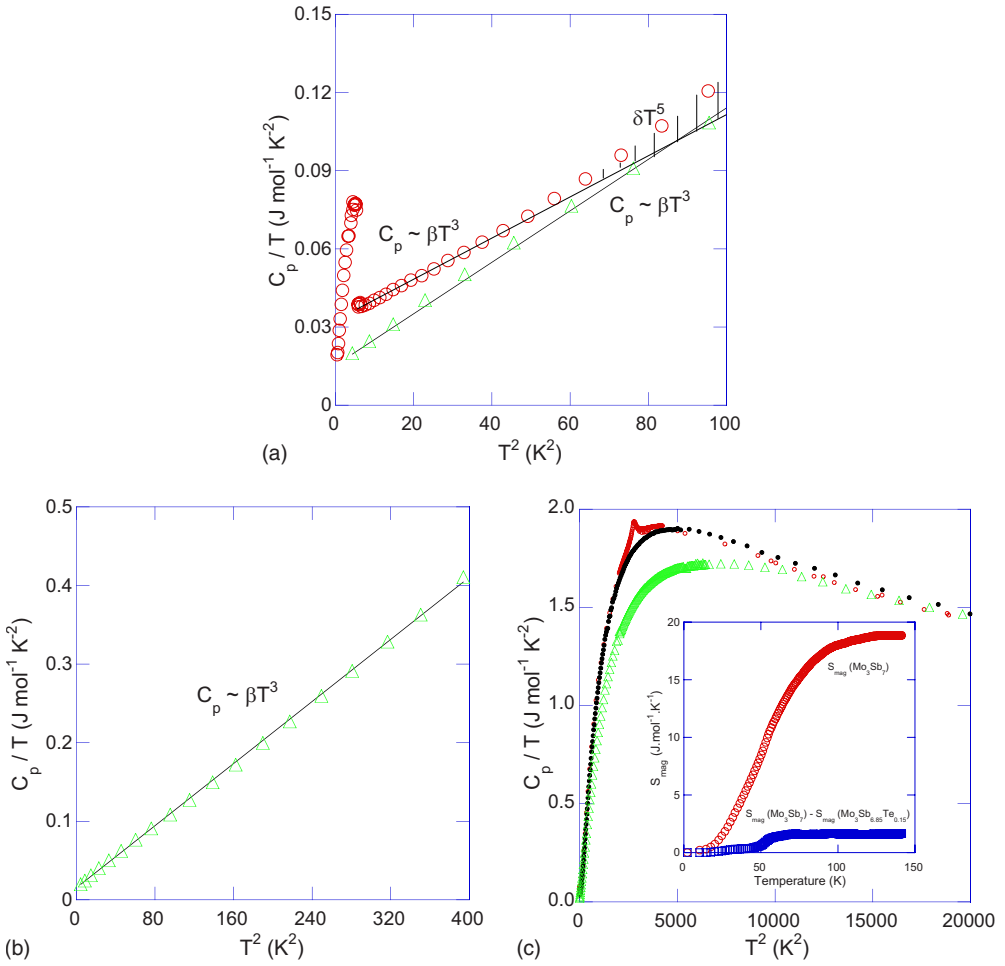

FIG. 6. (Color online) (a) Low-temperature specific heat for $x=0.0$ (○) and $x=1.6$ (△) as a function of T^2. The anharmonic contribution to the specific heat of the $x=0.0$ sample, and proportional to δT^5, is evidenced by the shaded area above the solid line. The specific heat jump exhibited by Mo_3Sb_7 is related to the superconducting transition at $T_c \sim 2.3$ K. (b) Low-temperature specific heat of the $x=1.6$ sample as a function of T^2 to highlight the broader temperature range where a linear dependence is observed. (c) Temperature dependence of the specific heat of the $x=0.0$ (○), 0.15 (●), and 1.6 (△) samples. Inset: Temperature dependence of the magnetic entropy S_{mag} of Mo_3Sb_7 (○), and of the difference between the magnetic entropy of Mo_3Sb_7 and of the $x=0.15$ compound.

$$C_p = \gamma T + \beta T^3 + \delta T^5, \tag{4}$$

where γT is the electronic contribution with γ as the Sommerfeld constant and $\beta T^3 + \delta T^5$ as the lattice contribution. The δT^5 term has been added to take into account the anharmonicity of the lattice. The values of the γ, β, and δ parameters are summarized in Table IV. As we can see, γ is strongly lowered for a high Te content. The decrease in γ may reflect the decrease in $N(E_F)$ with x as already evidenced by the magnetic-susceptibility data. Using the free-electron formula in the noninteracting limit $\gamma=0.173N(E_F)$, where γ and $N(E_F)$ are expressed in mJ mol^{-1} K^{-2} and states Ry^{-1} f.u.$^{-1}$, respectively, $N(E_F)$ can then be deduced (see Table IV). The obtained values constitute another piece of evidence in favor of a decrease in $N(E_F)$ with x, consistent with both band-structure calculations (Table II) and magnetic-susceptibility analyses. If we further assume that discrepancies between the experimental and theoretical values are mainly linked to the electron-phonon interactions, we can then roughly estimate the electron-phonon coupling constant $\lambda_{e\text{-ph}}$ using the relation $N(E_F)_{exp}/N(E_F)_{KKR\text{-}CPA}=1$

TABLE IV. Values of the γ, β, and δ parameters, and experimental total DOS values $N(E_F)_{exp}$ inferred from low-temperature specific-heat analyses.

Chemical formula	γ (mJ mol^{-1} K^{-2})	β (mJ mol^{-1} K^{-4})	δ (mJ mol^{-1} K^{-6})	$N(E_F)_{exp}$ (states Ry^{-1} f.u.$^{-1}$)
Mo_3Sb_7	34.2	0.65	2.6×10^{-3}	198
$Mo_3Sb_{5.4}Te_{1.6}$	16.3	0.95		94

$+\lambda_{e\text{-ph}}$, where $N(E_F)_{\text{exp}}$ and $N(E_F)_{\text{KKR-CPA}}$ are the experimental and theoretical KKR-CPA values of $N(E_F)$, respectively. We then obtained $\lambda_{e\text{-ph}} \sim 0.2$ for $x=1.6$. Based on the McMillan formula,[30] this value is too low to result in the appearance of a superconducting state in this material.

Alternatively to the magnetic-susceptibility data which suggest that samples with high Te contents no longer experience short-range interactions, specific-heat data may also provide further evidence for this evolution. Figure 6(c) depicts the specific heat, C_p/T, as a function of T^2 in the temperature region of interest (2–130 K) for the $x=0.0$ and $x=1.6$ samples. Because of the extreme sensitivity of the spin gap against Te concentration, we synthesized an additional sample with a lower Te content ($x=0.15$). The second-order phase transition associated in Mo_3Sb_7 with the spin gap formation can be clearly distinguished as a kink in the temperature dependence of C_p/T near 50 K, in perfect agreement with previous investigations.[14] Remarkably, a Te content as low as 0.15 is sufficient to suppress this anomaly. Such magnetic transition results in an additional contribution to the specific heat that can then be rewritten as

$$C_p = C_{\text{el}} + C_{\text{ph}} + C_{\text{mag}}, \tag{5}$$

where C_{el}, C_{ph}, and C_{mag} are the electronic, lattice, and magnetic contributions, respectively. It must be emphasized that the magnetic contribution is significantly suppressed below 20 K and, most likely, does not play a significant role in the aforementioned analysis.[14] To estimate this last magnetic term, we subtracted the electronic contribution deduced from the low-temperature specific-heat analysis ($C_{\text{el}}=\gamma T$) and the lattice contribution of the "non magnetic" $x=1.6$ sample to the specific-heat data of the $x=0.0$ and $x=0.15$ samples. Since Sb and Te display similar atomic radii and masses, no mass effect correction has been applied. The magnetic entropy, S_{mag}, has been then inferred by integration of the magnetic specific heat using the relation

$$S_{\text{mag}} = \int_0^T \frac{C_{\text{mag}}}{T'} dT'. \tag{6}$$

The inset of Fig. 6(c) illustrates the temperature dependence of S_{mag} of the $x=0.0$ and $x=0.15$ samples. In the case of Mo_3Sb_7, these results are in excellent agreement with those previously obtained by Tran *et al.*[14] S_{mag} saturates above 120 K to a limit value close to that expected for a second-order phase transition in a system of spins $\frac{1}{2}$ (R ln 2, where R is the molar gas constant). By slightly increasing the Te content, S_{mag} is shifted to lower values consistent with the magnetic-susceptibility data, i.e., with a picture, whereby magnetic interactions are progressively suppressed by increasing x. Therefore, the variation in the magnetic contribution to the specific heat further supports the idea that Te substitution drastically affects the low dimensional magnetism exhibited by Mo_3Sb_7.

E. Transport and magnetotransport properties

The electrical resistivity as a function of the temperature is shown in Fig. 7 for the various compounds synthesized.

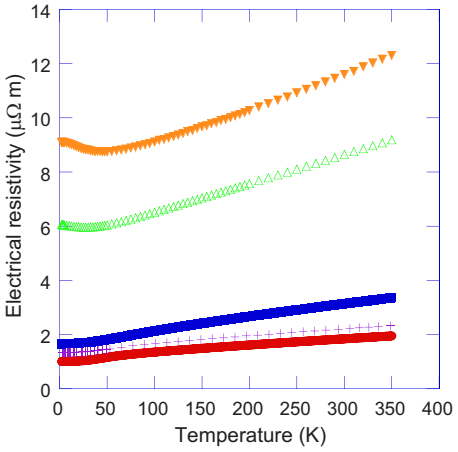

FIG. 7. (Color online) Temperature dependence of the electrical resistivity of the $Mo_3Sb_{7-x}Te_x$ compounds for $x=0.0$ (○), 0.3 (+), 1.0 (□), 1.6 (△), and 1.8 (▼).

None of the sample displays semiconductinglike electrical conduction. This first essential feature unambiguously shows that a crossover to semiconducting properties does not occur because of the too low Te content with regards to the required value. Moreover, the superconducting transition undergone by the Mo_3Sb_7 compound can no longer be distinguished by increasing x in the temperature range investigated, consistent with the specific-heat analysis.

As these measurements attest to, the partial substitution of Sb by Te has a strong impact on the electrical conduction since the electrical resistivity increases as the Te content becomes higher. While the temperature dependences of the electrical resistivity of the $x=0.3$ and 1.0 compounds exhibit common features with Mo_3Sb_7, i.e., a low-temperature activatedlike behavior and a transition from positive to negative curvature as the temperature increases, further enhancement of the Te concentration results in drastic changes. Actually, for $x=1.6$ and 1.8, the resistivity displays a minimum at 35 and 50 K, respectively, and above these temperatures, a linear dependence. These results are coherent with a rigidlike behavior of the electronic structure since an increase in the electrical resistivity arises as a consequence of the Fermi-

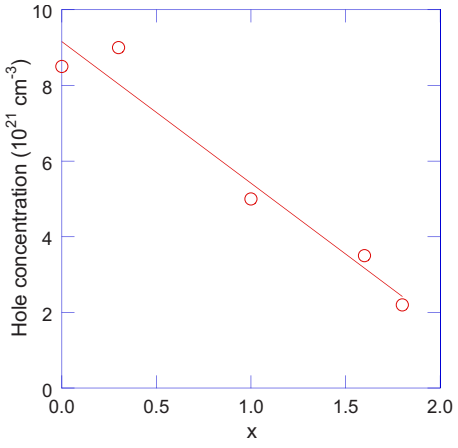

FIG. 8. (Color online) Hole concentration displayed as a function of the Te content.

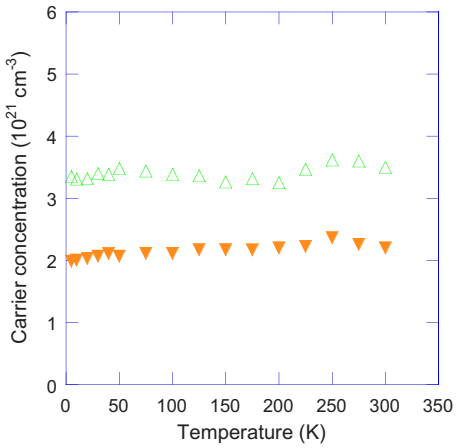

FIG. 9. (Color online) Carrier concentration of the $x=1.6$ (△) and 1.8 (▼) samples as a function of the temperature from 2 to 300 K.

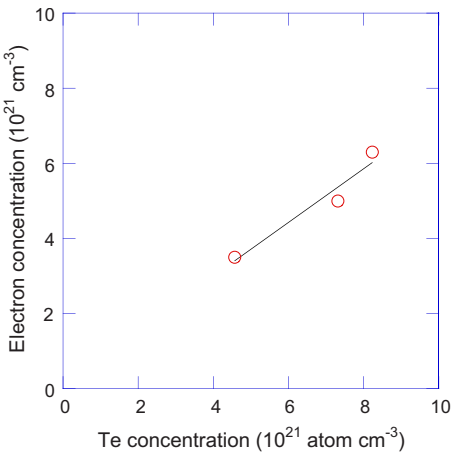

FIG. 10. (Color online) Electron concentration added to the structure as a function of the Te concentration.

level shift (see Figs. 2 and 3). Furthermore, if the salient features shared by the $x=0.0$, 0.3, and 1.0 samples have been interpreted as a possible indication of the presence of spin fluctuations in Mo_3Sb_7,[12] such a temperature dependence has also been underlined to be consistent with the formation of a spin gap near 50 K.[14] Thus, the disappearance of these characteristics with enhancing the Te content provides another experimental evidence of the suppression of the antiferromagnetic interactions displayed by Mo_3Sb_7. This viewpoint is also strongly supported by the low-temperature magnetotransport measurements.

Whatever the Te content is, all samples display a positive Hall coefficient, R_H, throughout the whole temperature range investigated, indicative of hole conduction. It must be mentioned that only information near room temperature has been obtained for the $x=0.0$, 0.3, and 1.0 samples. Actually, at lower temperature, the Hall resistance, ρ_H, shows strong variations with the magnetic-field strength which are presumably linked to the presence of these magnetic interactions.[21] This hypothesis is further corroborated by the data measured on both the $x=1.6$ and 1.8 samples for which the superlinear variation in ρ_H has disappeared together with the magnetic interactions.[21]

Assuming the presence of only one type of carriers and a parabolic dispersion relation, the hole concentration, p, can be estimated from the simple relation $p=1/R_He$. As evidenced by Fig. 8, the hole concentration linearly diminishes with x as expected from a rigidlike evolution of the electronic structure. For high Te contents, namely, $x=1.6$ and 1.8, the measured room-temperature values are consistent with those found by Gascoin *et al.*[11] for $x=1.5$ and 1.6. Furthermore, the hole concentrations of the $x=1.6$ and 1.8 samples are temperature-independent suggestive of a metalliclike behavior (Fig. 9) and further support the idea that a semiconducting state is far from being reached for these Te contents.

Not only does a crossover to semiconducting properties depend on a rigidlike behavior of the electronic structure but it is also intimately related to the tellurium atoms that are expected to donate one extra electron per atom to the valence band. To experimentally explore this assumption, we have plotted in Fig. 10 the number of electrons added in relation to the Te concentration. The electron concentration added to the structure increases quasilinearly with x. The slope of the line then leads to an estimation of the number of additional electrons per Te atom. In the present case, it amounts to ~0.75 electron per Te atom and is therefore, consistent with the theoretical value expected.

To settle the issue concerning the dominant scattering process of the charge carriers, we have calculated the Hall mobility, μ_H, defined as $\mu_H=R_H/\rho$, using both the measured Hall coefficient and the electrical resistivity values (Table V). These values are coherent with the rather high carrier concentrations displayed by these materials. Figure 11 shows

TABLE V. Hole concentration (p), Hall mobility (μ_H), Seebeck coefficient (α), electrical resistivity (ρ), and thermal conductivity (λ) measured at room temperature for the different $Mo_3Sb_{7-x}Te_x$ compounds studied.

Chemical formula	p (cm^{-3})	ϵ_H ($cm^2\ V^{-1}\ s^{-1}$)	α ($\mu V\ K^{-1}$)	ρ ($\mu\Omega$ m)	λ ($W\ m^{-1}\ K^{-1}$)
Mo_3Sb_7	8.5×10^{21}	4.1	18	1.8	6.2
$Mo_3Sb_{6.7}Te_{0.3}$	9.0×10^{21}	3.1	21	2.2	5.6
Mo_3Sb_6Te	5.0×10^{21}	4.0	34	3.1	5.1
$Mo_3Sb_{5.4}Te_{1.6}$	3.5×10^{21}	2.1	48	8.6	3.8
$Mo_3Sb_{5.2}Te_{1.8}$	2.2×10^{21}	2.4	60	11.7	4.5

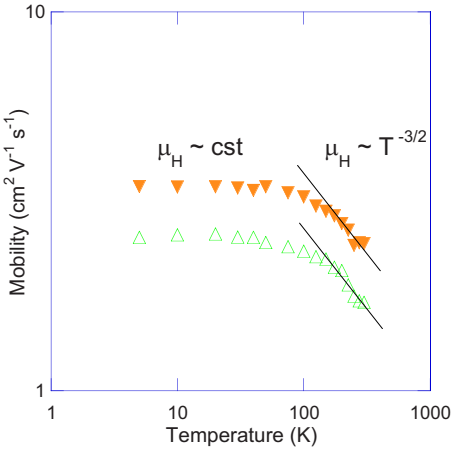

FIG. 11. (Color online) Temperature dependence of the Hall mobility μ_H of the $x=1.6$ (△) and 1.8 (▼) samples.

the temperature dependence of μ_H for the $x=1.6$ and 1.8 compounds. Below 100 K, the Hall mobilities are constant suggestive of holes scattered by neutral impurities. Above this temperature, the mobility varies following a law close to $T^{-3/2}$ characteristic of hole scattering by acoustic phonons.

Figure 12 depicts the temperature dependence of the thermopower α of the $Mo_3Sb_{7-x}Te_x$ compounds. For all samples, the Seebeck coefficient is positive, indicative of p-type conduction, and therefore confirms the results obtained from the magnetotransport study. Addition of tellurium results in a progressive decrease in the carrier concentration, which, in turn, increases the magnitude of α. The thermopower values are in very good agreement with those obtained in previous studies and are coherent with our theoretical estimation of α using the Mott's formula.[10,11] In addition to the diffusive thermopower revealed by the linear temperature dependence above 100 K, a slight curvature can be distinguished at low temperature for all samples. Such feature is usually related to a drag effect. Since none of these compounds exhibit a magnetic ordering, a magnon-drag effect can be ruled out. Thus, a phonon drag seems to provide the most straightforward explanation for the observed behavior in the present case.

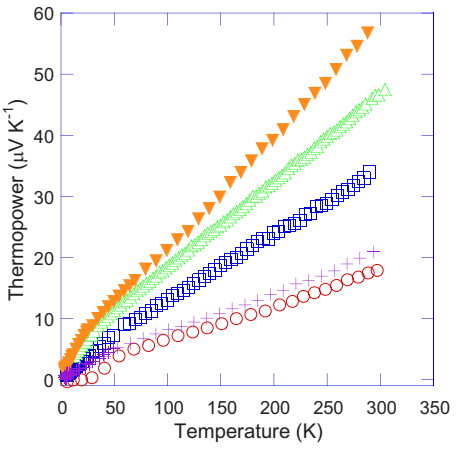

FIG. 12. (Color online) Temperature dependence of the thermopower of the $Mo_3Sb_{7-x}Te_x$ compounds for $x=0.0$ (○), 0.3 (+), 1.0 (□), 1.6 (△), and 1.8 (▼).

TABLE VI. Effective masses (m^*/m_0), reduced Fermi level (η), and Lorenz number (L) estimated from Eqs. (7), (8), and (11).

Chemical formula	m^*/m_0	η	L ($\times 10^{-8}$ V^2 K^{-2})
Mo_3Sb_7	3.7	15.8	2.40
$Mo_3Sb_{6.7}Te_{0.3}$	4.5	13.5	2.39
Mo_3Sb_6Te	4.9	8.4	2.33
$Mo_3Sb_{5.4}Te_{1.6}$	5.4	5.9	2.23
$Mo_3Sb_{5.2}Te_{1.8}$	5.0	4.6	2.15

Alternatively to the magnetic approach, the hole reduced effective masses, m^*/m_0, of the Te substituted samples can be numerically estimated at room temperature by assuming a single parabolic-band model and using the experimental values of the thermopower and carrier concentration. The Hall mobility study indicates that acoustic phonons can be considered as the most prominent scatters of the charge carriers near room temperature in the $x=1.6$ and 1.8 compounds leading to the following expressions for the thermopower and the hole concentration[1]

$$\alpha = -\frac{k_B}{e}\left(\frac{2F_1(\eta)}{F_0(\eta)} - \eta\right), \tag{7}$$

$$p = \frac{4}{\sqrt{\pi}}\left(\frac{2\pi m^* k_B T}{h^2}\right)^{3/2} F_{1/2}(\eta), \tag{8}$$

where F_i is the Fermi integral of order i, η is the reduced Fermi level defined as $\eta = E_F/k_BT$, k_B is the Boltzmann constant, h is the Planck constant, and e is the elementary charge. Assuming that acoustic phonon scattering is the most prominent scattering mechanism at play in these materials whatever the Te content is, the reduced effective masses m^*/m_0 and Fermi levels η were deduced from these above-mentioned equations, and are summarized in Table VI for all samples. The enhanced m^*/m_0 values are in fair agreement with those derived from the magnetic-susceptibility data (Table III) given the underlying hypothesis of these two approaches. Nevertheless, both methods lead to quasiconstant values with x. The obtained η values provide additional evidence in favor of a shift of the Fermi level toward the valence-band edge as x increases and demonstrate the high degree of degeneracy displayed by these compounds. Therefore, η values show that Fermi-Dirac statistics are no longer required, and Eqs. (7) and (8) can then be simplified to obtain the carrier-concentration dependence of the thermopower[31]

$$\alpha = \frac{8\pi^2 k_B^2}{3eh^2} m^* T\left(\frac{\pi}{3p}\right)^{2/3}. \tag{9}$$

As Fig. 13 attests to, the experimental values of the thermopower follow this trend. A fit of the data according to relation (9) results in an experimental exponent of ~−0.8 that coupled with quasiconstant effective masses testifies to the ability of metallic equations to describe this system.

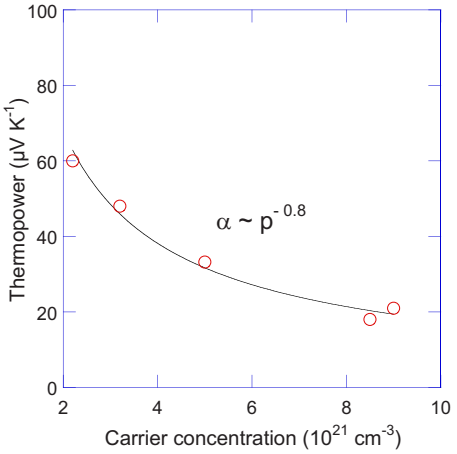

FIG. 13. (Color online) Seebeck coefficient measured at room temperature as a function of the carrier concentration. The solid line stands for the best fit to the data according to relation (9). Note that a fit without the $x=0.3$ data point would lead to an exponent of ~ -0.9.

The total thermal conductivity as a function of the temperature is presented in Fig. 14(a). All the data have been corrected to take into account the relative density of the different samples.[32] As we can observe, the minimum near 53 K, which characterizes Mo_3Sb_7 and that is attributed to the spin gap formation,[21] is strongly lessened in the $x=0.3$ sample. This evolution seems to indicate that the spin gap and the dimerization process are progressively, rather than abruptly, destroyed by this partial substitution. The disappearance of this minimum together with the spin gap when x is further increased constitutes a compelling evidence in favor of a close relationship between these two characteristics as previously suggested.[21] However, the most striking outcome of these measurements is the obvious increase in the thermal conductivity at low temperature as the Te concentration increases. To try to shed light on this behavior, we have estimated the lattice part of the total thermal conductivity by subtracting the carrier thermal conductivity according to the Wiedemann-Franz law

$$\lambda_e = \frac{LT}{\rho}, \tag{10}$$

where T is the absolute temperature and L is the Lorenz number. The aforementioned analysis of the degree of degeneracy indicates that these samples can be considered as highly degenerate. Thus, fixing L to the value of a degenerate electron gas, i.e., $L=L_0=2.44\times10^{-8}$ V^2 K^{-2}, should constitute a good approximation. To ascertain this last hypothesis, the Lorenz number can be estimated from the following equation[33]

$$L = \left(\frac{k_B}{e}\right)^2 \left\{ \frac{\left(s+\frac{7}{2}\right)F_{s+(5/2)}(\eta)}{\left(s+\frac{3}{2}\right)F_{s+(1/2)}(\eta)} - \left[\frac{\left(s+\frac{5}{2}\right)F_{s+(3/2)}(\eta)}{\left(s+\frac{3}{2}\right)F_{s+(1/2)}(\eta)} \right]^2 \right\}, \tag{11}$$

where $s=-1/2$, $s=0$, and $s=3/2$ stand for acoustic phonon, neutral impurity, and ionized impurity scatterings, respectively. As already mentioned, the temperature dependence of the Hall mobilities has suggested that acoustic phonons constitute the main scatters in the $x=1.6$ and 1.8 samples. Therefore, taking $s=-1/2$ and using the values of the reduced Fermi level derived from Eq. (7), the Lorenz number can then be calculated (Table VI). As can be observed, only slight discrepancies exist between these values and L_0, and thus, further corroborate the relatively large degree of degeneracy displayed by these compounds.

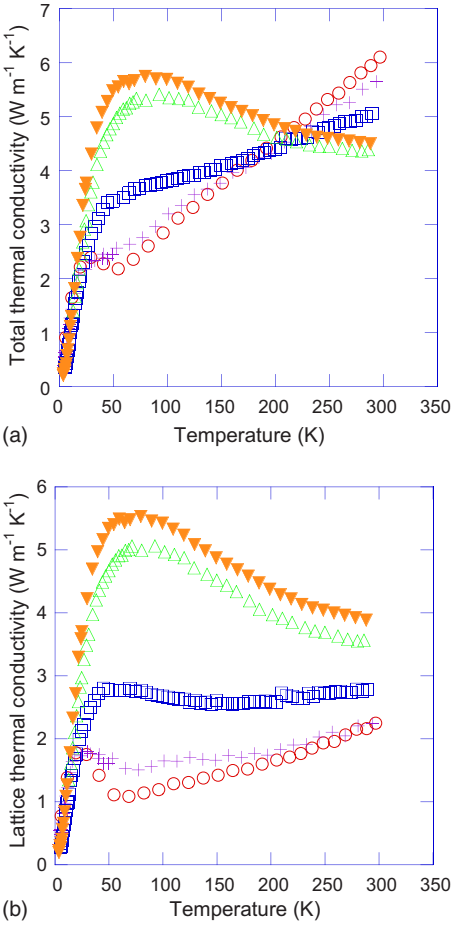

FIG. 14. (Color online) Temperature dependence of the total thermal conductivity (a) and of the lattice thermal conductivity (b) for $x=0.0$ (○), 0.3 (+), 1.0 (□), 1.6 (△), and 1.8 (▼).

As Fig. 14(b) shows, the lattice thermal conductivity progressively increases below 150 K upon substituting antimony by tellurium. Slight differences in the microstructure (i.e., grain size) or related to the metallurgical route cannot explain such differences. Moreover, we believe that the electron-phonon interactions exhibited by the Mo_3Sb_7 compound and its depression with increasing Te concentration cannot solely constitute a satisfying explanation. To account for such an increase in the phononic part of the thermal conductivity, although disorder in the crystalline structure increases with Te content, an overriding scattering mechanism should be lowered by increasing x. The magnetic interactions displayed by Mo_3Sb_7 which originates from magnetically frustrated lattice with predominantly antiferromagnetically coupled molybdenum dimers could then provide a fruitful picture. Actually, the variation in the electrical resistivity

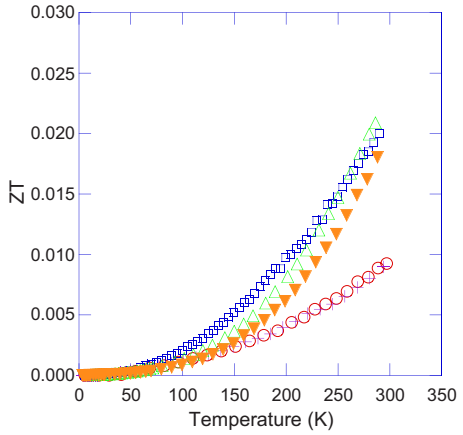

FIG. 15. (Color online) Temperature dependence of the dimensionless figure of merit ZT of the $x=0.0$ (○), 0.3 (+), 1.0 (□), 1.6 (△), and 1.8 (▼) compounds.

with the Te concentration, the absence of a minimum in the thermal-conductivity temperature dependence, and the variation in the magnetic susceptibility with x are consistent with a progressive suppression of these interactions by Te substitution. In the case of Mo_3Sb_7, the dimer-phonon interactions seem to be the dominant scattering source responsible for the observed exotic temperature dependence of the thermal conductivity.[21] As a consequence, if the strength of this mechanism is strongly lowered, the lattice thermal conductivity should increase. Thus, this picture seems to be consistent with our experimental results, which in turn, may reinforce the scenario proposed for the Mo_3Sb_7 compound.

Based on the results of the thermoelectric properties, the dimensionless figure of merit, ZT, can be calculated for the Te substituted compounds (Fig. 15). For all samples, the ZT values increase with both increasing temperature and Te concentration. A maximum ZT value of 0.02 was achieved near room temperature for $x=1.6$.

IV. SUMMARY

We have presented experimental and theoretical investigations of low-temperature transport and magnetic properties in some $Mo_3Sb_{7-x}Te_x$ compounds with $x=0.0$, 0.3, 1.0, 1.6, and 1.8 using thermopower, thermal conductivity, electrical resistivity, magnetic susceptibility, Hall effect, specific-heat measurements, as well as electronic band-structure calculations.

The partial substitution of antimony by tellurium drastically affects the transport properties of Mo_3Sb_7. Even though the solubility limit of Te precludes a metal-insulator transition, the magnitude of both the thermopower and the electrical resistivity increases with x. In addition, the transport data were found to be consistent with our theoretical KKR-CPA analysis, i.e., with a picture, whereby the evolution of the electronic structure can be understood within a rigid-band model. Introducing tellurium in the structure leads to a progressive suppression of the magnetic interactions displayed by the Mo_3Sb_7 compound. Compelling experimental evidence of this disappearance has been provided by magnetic-susceptibility measurements as well as specific-heat analysis. The suppression of the low dimensional magnetism and the concomitant uncommon increase in the lattice thermal conductivity with x strongly suggest that these magnetic interactions do play a crucial role on the thermal conduction processes. Specific-heat analysis revealed a decrease in both the electron-phonon coupling constant and the density of states at the Fermi level which is in perfect agreement with our transport data and band-structure calculations, respectively.

ACKNOWLEDGMENTS

The authors warmly thank E. Šantavá for specific-heat measurements and C. Bellouard for magnetotransport measurements. C.C. greatly thanks M. Amiet and P. Maigné, and financial support of DGA (Délégation Générale pour l'Armement, Ministry of Defense, France) and the European Network of Excellence CMA (Complex Metallic Alloys). J.H. acknowledges the financial support of the Czech Science Foundation (Grant No. 203/09/1036). J.T. acknowledges the partial support of the Polish Ministry of Science and Higher Education (Grants No. N202-2104-33 and No. 44/N-COST/2007/0).

*Corresponding author; candolfi@mines.inpl-nancy.fr
†Present address: Max-Planck-Institut für Chemische Physik fester Stoffe, Nöthnitzer Str. 40, 01187 Dresden, Germany; candolfi@cpfs.mpg.de

[1] H. J. Goldsmid, *Thermoelectric Refrigeration* (Temple Press Books Ltd, London, 1964).
[2] G. Slack, in *CRC Handbook of Thermoelectrics*, edited by D. M. Rowe (CRC, Boca Raton, FL, 1995).
[3] G. S. Nolas, M. Kaeser, R. T. Littleton IV, and T. M. Tritt, Appl. Phys. Lett. **77**, 1855 (2000).
[4] B. C. Sales, D. Mandrus, and R. K. Williams, Science **272**, 1325 (1996).
[5] C. Uher, in *Semiconductors and Semimetals*, edited by T. Tritt (Academic Press, San Diego, 2000), Vol. 69, p. 139.
[6] G. S. Nolas, G. A. Slack, and S. B. Shujman, in *Semiconductors and Semimetals*, edited by T. Tritt (Academic Press, San Diego, 2000), Vol. 69, p. 255.
[7] S. M. Kauzlarich, S. R. Brown, and G. J. Snyder, Dalton Trans. **2007**, 2099.
[8] U. Häussermann, M. Elding-Ponten, C. Svensson, and S. Lidin, Chem.-Eur. J. **4**, 1007 (1998).
[9] A. Brown, Nature (London) **206**, 502 (1965).
[10] E. Dashjav, A. Szczepenowska, and H. Kleinke, J. Mater. Chem. **12**, 345 (2002).
[11] F. Gascoin, J. Rasmussen, and G. J. Snyder, J. Alloys Compd. **427**, 324 (2007).
[12] C. Candolfi, B. Lenoir, A. Dauscher, C. Bellouard, J. Hejtmanek, E. Santava, and J. Tobola, Phys. Rev. Lett. **99**, 037006 (2007).

[13] C. Candolfi, B. Lenoir, A. Dauscher, J. Hejtmanek, E. Santava, and J. Tobola, Phys. Rev. B **77**, 092509 (2008).
[14] V. H. Tran, W. Miiller, and Z. Bukowski, Phys. Rev. Lett. **100**, 137004 (2008).
[15] Z. Bukowski, D. Badurski, J. Stepien-Damm, and R. Troc, Solid State Commun. **123**, 283 (2002).
[16] R. Khasanov, P. W. Klamut, A. Shengelaya, Z. Bukowski, I. M. Savic, C. Baines, and H. Keller, Phys. Rev. B **78**, 014502 (2008).
[17] T. Koyama, H. Yamashita, Y. Takahashi, T. Kohara, I. Watanabe, Y. Tabata, and H. Nakamura, Phys. Rev. Lett. **101**, 126404 (2008).
[18] A. B. Karki, D. P. Young, P. W. Adams, E. K. Okudzeto, and Julia Y. Chan, Phys. Rev. B **77**, 212503 (2008).
[19] B. Wiendlocha, J. Tobola, M. Sternik, S. Kaprzyk, K. Parlinski, and A. M. Oles, Phys. Rev. B **78**, 060507(R) (2008).
[20] V. H. Tran, W. Miiller, and Z. Bukowski, Acta Mater. **56**, 5694 (2008).
[21] C. Candolfi, B. Lenoir, A. Dauscher, E. Guilmeau, J. Hejtmanek, J. Tobola, B. Wiendlocha, and S. Kaprzyk, Phys. Rev. B **79**, 035114 (2009).
[22] N. Soheilnia, H. Xu, H. Zhang, T. M. Tritt, I. Swainson, and H. Kleinke, Chem. Mater. **19**, 4063 (2007).
[23] J. Korringa, Physica (Utrecht) **13**, 392 (1947); W. Kohn and N. Rostoker, Phys. Rev. **94**, 1111 (1954).
[24] A. Bansil, S. Kaprzyk, P. E. Mijnarends, and J. Tobola, Phys. Rev. B **60**, 13396 (1999), and references therein.
[25] C. Candolfi, B. Lenoir, A. Dauscher, J. Tobola, S. J. Clarke, and R. I. Smith, Chem. Mater. **20**, 6556 (2008).
[26] T. Stopa, J. Tobola, S. Kaprzyk, E. K. Hlil, and D. Fruchart, J. Phys.: Condens. Matter **18**, 6379 (2006).
[27] P. Jensen, A. Kjekshus, and T. Skansen, Acta Chem. Scand. **20**, 403 (1966).
[28] L. N. Mulay and E. A. Boudreaux, *Theory and Applications of Molecular Diamagnetism* (John Wiley and Sons, New York, 1976).
[29] S. V. Vonsovskii, *Magnetism* (John Wiley and Sons and Keter Jerusalem Publishing House Ltd, New York, 1974), Vol. 1.
[30] W. L. McMillan, Phys. Rev. **167**, 331 (1968).
[31] M. Cutler, J. F. Leavy, and R. L. Fitzpatrick, Phys. Rev. **133**, A1143 (1964).
[32] R. Landauer, J. Appl. Phys. **23**, 779 (1952).
[33] *Thermoelectric Materials and Devices* (Reinhold, New York, 1960).